In Situ Observation of the Formation of Fe_3O_4 in Fe_4N (001) due to Electron Irradiation

Z. Q. Liu,[1,*] H. Hashimoto,[2] E. Sukedai,[2] M. Song,[1] K. Mitsuishi,[1] and K. Furuya[1]

[1]*Nanomaterials Laboratory, National Institute for Materials Science, Tsukuba 305-0003, Japan*

[2]*Department of Mechanical Engineering, Okayama University of Science, Okayama 700-0005, Japan*

(Received 30 January 2003; published 27 June 2003)

γ'-Fe_4N was subjected to electron irradiation with the dose rate of $6.8 \times 10^{23} e\ m^{-2}\ s^{-1}$ in a 400 kV transmission electron microscope. The first *in situ* observation of the formation of Fe_3O_4 (O) on Fe_4N (γ') with the orientation relationship of $\{100\}_O \parallel \{100\}_{\gamma'}$ and $\langle 001\rangle_O \parallel \langle 001\rangle_{\gamma'}$ has been made inside the microscope with the basic column vacuum of $(5–6) \times 10^{-5}$ Pa. A mechanism is proposed involving the electron-stimulated dissociation of Fe-N chemical bonds, desorption of nitrogen from the surface, adsorption of oxygen to the surface, and the oxidization of excessive metallic iron on the surface.

DOI: 10.1103/PhysRevLett.90.255504 PACS numbers: 61.82.Bg, 61.80.Fe, 68.37.Lp, 73.20.At

Growing interest has been prompted in the investigation of Fe_3O_4 (magnetite) as an important material in catalysis, corrosion, geochemistry, and magnetism. The preparation of Fe_3O_4 plays a key role in this field of research and much literature has reported the growing of Fe_3O_4 crystals on Pt [1–4], MgO [5–8], and Al_2O_3 [9] substrates with different methods. Regarding the crystallographic properties, Fe_4N nitride might not be a good candidate for preparing Fe_3O_4 oxide, between which the lattice mismatch is up to 10%. In addition, many investigations have been devoted to the study of electron-stimulated oxidization of metallic surfaces [10–14] and semiconductor surfaces [15,16] that were exposed to oxygen atmosphere, but little attention has been paid to those occurring in the high-vacuum system of electron microscopes with low oxygen partial pressure [17]. In this Letter we first report the formation of Fe_3O_4 on Fe_4N due to electron beam irradiation under high-vacuum conditions in transmission electron microscope (TEM), which suggests a new method to prepare local Fe_3O_4 crystal within Fe_4N film by selective electron beam irradiation, noting that both of them are good magnetic materials with many utilities.

Fe_4N iron nitride used in this study came from the ion nitriding of polycrystalline pure iron at 823 K for 4 h in a gas mixture of NH_3 and 10% CH_3COCH_3 under a pressure of 800–930 Pa. The transition compound sublayer, which is mainly made up of equiaxed Fe_4N grains, was selected for this study to prepare TEM specimens using ion milling with the process described elsewhere [18]. Before a brief through-air transfer to the TEM chamber the surface of the specimen was cleaned again by a 3 kV Ar ion beam for 10 min with 4° inclined to the surface. An electron microscope with basic column vacuum pressure of $(5–6) \times 10^{-5}$ Pa was used to carry out the investigation at an accelerating voltage of 400 kV. In order to observe the initial stage of the specimen, Fe_4N grain in the [001] orientation was selected as soon as possible to record its initial diffraction pattern, which was defined as the starting point of the electron irradiation. All observations were carried out with a beam current around 11 $A\,cm^{-2}$ on specimen, which corresponds to a dose rate of $6.8 \times 10^{23} e\ m^{-2}\ s^{-1}$. The diffraction patterns and high resolution electron microscopy (HREM) images were *in situ* observed at room temperature with the increasing of electron beam irradiation time.

Figure 1 shows the [001] electron diffraction patterns of a γ'-Fe_4N grain irradiated by 400 KeV electrons for a different time as indicated in the bottom left corner. A perfect $[001]_{\gamma'}$ diffraction pattern was presented in Fig. 1(a) before irradiation, showing the ordering of a nitrogen atom at the octahedral interstice of the face-centered cubic (fcc) iron-atom sublattice. The $\pm(200)_{\gamma'}$, $\pm(020)_{\gamma'}$, and $\pm(220)_{\gamma'}$ big spots came from the fcc iron sublattice while the $\pm(100)_{\gamma'}$, $\pm(010)_{\gamma'}$, $\pm(110)_{\gamma'}$, and other relative small spots resulted from the ordering of the nitrogen atom in the iron-atom sublattice. After 16 min irradiation extra weak spots appeared inside the $\pm(110)_{\gamma'}$, $\pm(200)_{\gamma'}$, $\pm(020)_{\gamma'}$, and $\pm(220)_{\gamma'}$ spots in the diffraction pattern of Fig. 1(b) where some extra spots were indicated by arrowheads. The intensity of nitrogen-ordering-related small spots [e.g., $\pm(100)_{\gamma'}$, $\pm(010)_{\gamma'}$, and $\pm(110)_{\gamma'}$] decreased while that of extra spots increased after 64 min irradiation as shown in Fig. 1(c). After 123 min irradiation the nitrogen-ordering-related spots almost disappeared, but the extra spots indicated with arrowheads became sharp and strong as shown in Fig. 1(d). Despite the diffusion, the iron-sublattice spots [e.g., $\pm(200)_{\gamma'}$, $\pm(020)_{\gamma'}$, and $\pm(220)_{\gamma'}$] of Fe_4N nitride almost did not change during irradiation. Therefore, according to the crystal parameters of Fe_4N ($a = 0.3795$ nm) [19], the planar spacing of the extra spots could be calculated, which shows good agreement with the structure of the Fe_3O_4 oxide. The kinetically simulated electron diffraction patterns of Fe_4N and Fe_3O_4 structures along [001] orientation were shown in Figs. 1(e) and 1(f), respectively. It can be seen that the arrangement of the arrowhead-indicated extra spots, induced by electron irradiation in Fig. 1(d), coincides with the simulated pattern of Fe_3O_4 in Fig. 1(f) very well. The overlapping of Fig. 1(e) (Fe_4N) and Fig. 1(f) (Fe_3O_4) gives the exact spot configuration in Figs. 1(b) and 1(c). Thus

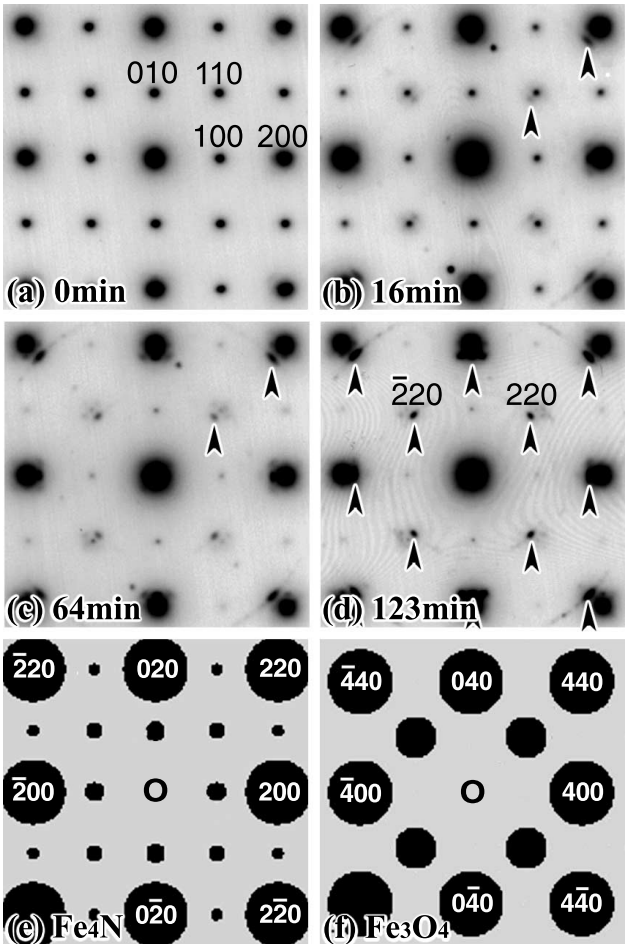

FIG. 1. (a) [001] diffraction pattern of Fe_4N showing clearly the nitrogen-ordering-related spots [e.g., $\pm(100)_{\gamma'}$] and the iron-sublattice-related spots [e.g., $\pm(200)_{\gamma'}$]. (b) Extra spots appear inside the $\pm(110)_{\gamma'}$ and $\pm(200)_{\gamma'}$ spots after 16 min irradiation. (c) Diffraction pattern after 64 min irradiation showing the decreasing intensity of nitrogen-ordering-related spots and the increasing intensity of extra spots. (d) Diffraction pattern after 123 min irradiation. Extra spots marked by arrowheads are indexed with Fe_3O_4 structure. (e) Kinetically simulated [001] diffraction pattern of Fe_4N in which the iron-sublattice-related spots are indexed. (f) Kinetically simulated [001] diffraction pattern of Fe_3O_4 showing good agreement with the marked extra spots in (d).

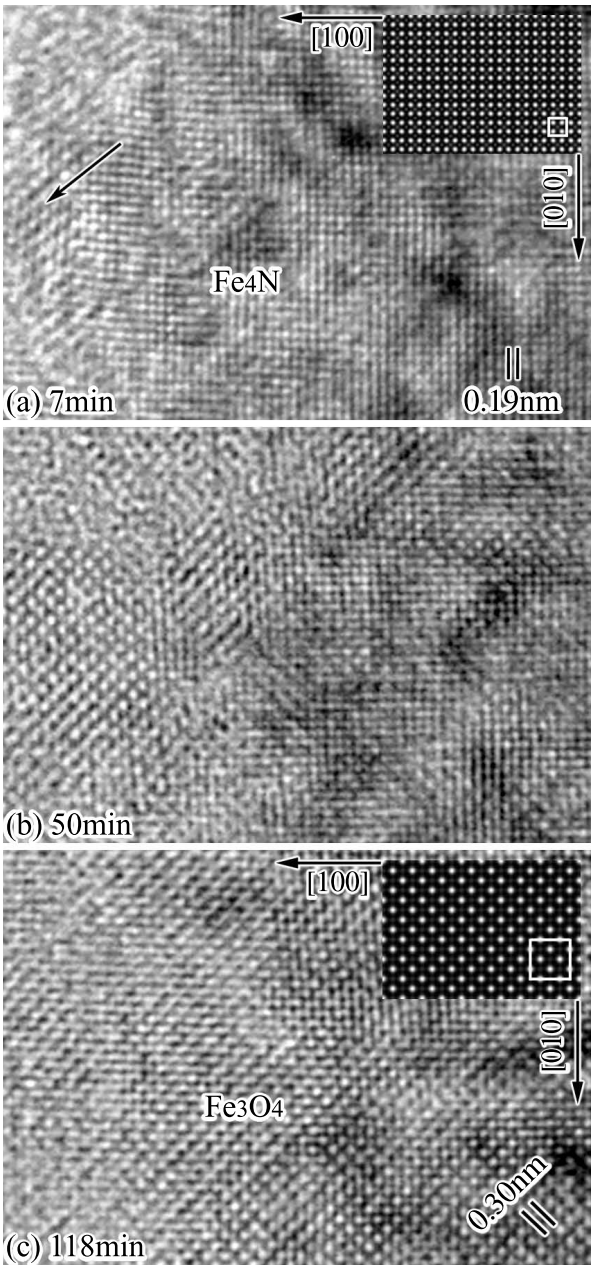

FIG. 2. (a) HREM image of Fe_4N [001] after 7 min irradiation showing the contrast line along the $[110]_{\gamma'}$ direction at the left thin area of the specimen. Inset is its simulated image with Scherzer defocus (40.5 nm) at the thickness of 4.175 nm. (b) HREM image after 50 min irradiation where a big square image with spacing of about 0.30 nm appears at the left thin area. (c) HREM image of Fe_3O_4 transformed from Fe_4N after 118 min electron irradiation. The simulated image (defocus 40.5 nm, thickness 4.198 nm) is inserted at the top right corner with marked structural unit, which shows good agreement with the observed image.

the extra spots were indexed with the Fe_3O_4 structure as shown in Fig. 1(d).

The *in situ* HREM observation of this process was also carried out at the same time, and some images were presented in Fig. 2. The left-hand side is the thin edge area of a hole in TEM foil while the right-hand side is the thick area in the specimen. Figure 2(a) is the HREM image recorded 7 min later than the diffraction pattern of Fig. 1(a) (defined as the starting point of electron beam irradiation). The original $(200)_{\gamma'}$ and $(020)_{\gamma'}$ planes of Fe_4N with the spacing of about 0.19 nm were shown clearly in this image. However, abnormal contrast appeared along the $[110]_{\gamma'}$ direction indicated by the arrow, especially at the left thin area. After 50 min irradiation in Fig. 2(b), the contrast lines appeared in both the $[110]_{\gamma'}$ and $[1\bar{1}0]_{\gamma'}$ directions, and a big square image was formed in the left thin area. Such an image extended into

the thick region as the prominent image after 118 min irradiation as shown in Fig. 2(c). This image was identified as the HREM image of Fe_3O_4 in [001] orientation, showing a square array of {220} lattice fringes with a spacing of about 0.30 nm. The simulated images of Fe_4N and Fe_3O_4 crystals along the [001] orientation were inserted in the top right corners of Figs. 2(a) and 2(c), respectively. These images were calculated under the Scherzer defocus (40.5 nm) of the microscope at the thickness of 4.175 nm for Fe_4N and 4.198 nm for Fe_3O_4, respectively. Good agreement has been shown between the observed and the simulated images for Fe_4N [Fig. 2(a)] and Fe_3O_4 [Fig. 2(c)] crystals. The corresponding structural unit cell was also shown with white squares at the bottom right corner of each inset. It was concluded that Fe_4N iron nitride transformed to Fe_3O_4 iron oxide due to electron beam irradiation under high-vacuum conditions in electron microscope. According to the diffraction patterns in Fig. 1 and the HREM images in Fig. 2, the orientation relationship between the formed Fe_3O_4 oxide (O) and the Fe_4N substrate (γ') was determined as $(100)_O \parallel (100)_{\gamma'}$ and $[001]_O \parallel [001]_{\gamma'}$.

It was observed that the transformation mentioned above can take place rapidly from the very beginning stage of electron irradiation. Figure 3(a) shows a HREM image just after 7 min electron irradiation, in which the left-hand side is the thin area while the right-hand side is the thick area of the specimen. Figure 3(a′) is its fast Fourier transform (FFT) image where the spots of Fe_4N nitride are presented as shown in the diffraction pattern of Fig. 1(a). However, the $\pm(400)$ and $\pm(040)$ spots of Fe_3O_4 (marked by counterclockwise arrowheads) have appeared inside the $\pm(200)_{\gamma'}$ and $\pm(020)_{\gamma'}$ spots (marked by clockwise arrowheads), which indicate the formation of Fe_3O_4 on the surface of Fe_4N. The outer Fe_4N {200} group spots and the inner Fe_3O_4 {400} group spots were separately selected with a suitable aperture in Figs. 3(b′) and 3(c′), and then were processed with inverse FFT to get the images of Figs. 3(b) and 3(c), respectively. Comparing these two images, the existence of Fe_3O_4 at the left thin area can be qualitatively verified. The boundary of the Fe_3O_4 island is roughly indicated by dots in Fig. 1(a). The image processing we used here, which involves the FFT of micrograph, the selective filtering, and the inverse FFT, also suggests an effective method to identify different phases in one micrograph.

Various aspects of the electron irradiation effect on the surface, such as adsorption, desorption, diffusion, and dissociation, have already been discussed in the literature. However, there is no accepted generalized theory of the electron irradiation effect since different systems demand individual consideration for each case. In our case, the significant changes observed in the diffraction patterns (see Fig. 1) are the disappearing of nitrogen-ordering-related spots, the diffusing of iron-sublattice-related spots, and the appearing of Fe_3O_4 spots in the diffraction pattern, while the changes in HREM image s(see Fig. 2)

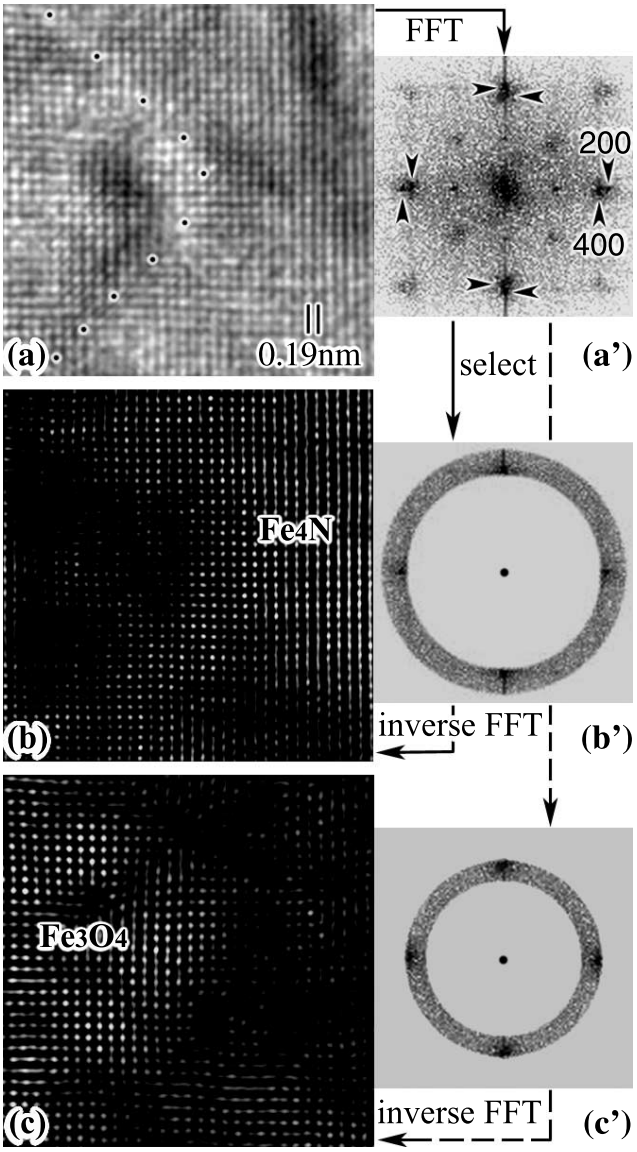

FIG. 3. Image processing revealing the formation of Fe_3O_4 crystal. (a) HREM image after 7 min irradiation where the left-hand side is the thin area of the specimen. The boundary of the Fe_3O_4 island is roughly indicated with dots. (a′) The FFT image of (a) showing both spots of Fe_3O_4 and Fe_4N. The {200} group spots of Fe_4N are marked with clockwise arrowheads, and the {400} group spots of Fe_3O_4 are marked with counterclockwise arrowheads. (b) The inverse FFT image of (b′) showing the iron sublattice in Fe_4N. (b′) The filtering image of (a′) with selection of {200} group spots of Fe_4N. (c) The inverse FFT image of (c′) showing the corresponding sublattice in Fe_3O_4. (c′) The filtering image of (a′) with selection of {400} group spots of Fe_3O_4.

include the appearing of contrast lines along the $\langle 110\rangle_{\gamma'}$ direction in the Fe_4N HREM image, the formation of the Fe_3O_4 image at the thin area, and the extension of the Fe_3O_4 image to the thick area. Considering the observed results mentioned above, a mechanism of the formation of Fe_3O_4 oxide in Fe_4N nitride is proposed involving the decomposition of Fe_4N nitride and the oxidization

for Fe_3O_4 oxide. We believe that the Fe_4N nitride was decomposed and nitrogen was desorbed into the high vacuum, which resulted in the disappearance of nitrogen-ordering-related spots in the diffraction pattern. There is also a possibility that the nitrogen atom randomly distributes among the iron sublattice in a disordered manner without depletion from the specimen. However, considering the subsequent accommodation and ordering of oxygen atoms, it is impossible for the well-ordered Fe_3O_4 structure to accommodate the disordered nitrogen atoms in between, which improves the whole energy of the system. In contrast to the desorption of nitrogen, oxygen was simultaneously adsorbed into the specimen to oxidize the surface metallic iron rapidly. Thus the basic unit of the iron sublattice shrinks when nitrogen goes out of the specimen and expands when oxygen goes into the specimen, resulting in the diffusion of iron-sublattice-related spots in the diffraction pattern. The role of the electron beam in the decomposition of Fe_4N is to break Fe-N chemical bonds and then stimulate the desorption of nitrogen, while in the oxidation process it acts to stimulate the adsorption and ionization of oxygen to oxidize the excessive iron with the mechanism reported on Si [11], Al [13,14], and Fe [20] surfaces. The similar process due to electron irradiation has been observed in the oxidization of InP in a UHV chamber, which includes the dissociation of In-P chemical bonds, depletion of phosphorus, and oxidization of metallic indium [17]. Considering that both nitrogen and phosphorus belong to the same family in the element period table, it is not surprising to find that they have similar behavior under electron irradiation.

As far as we know, Fe_4N is a metastable phase with respect to decomposition into N_2 gas and α-Fe (with very low N content). Its standard Gibbs free energy of formation is $+3.8$ KJ/mol, whereas that of Fe_3O_4 is -1015.4 KJ/mol. Thus from a thermodynamical point of view it is not surprising to observe that Fe_4N iron nitride transformed to Fe_3O_4 iron oxide in our work. Among different iron oxides, e.g., FeO, Fe_3O_4, α-Fe_2O_3, and γ-Fe_2O_3, only Fe_3O_4 was formed in Fe_4N as detected in diffraction patterns (see Fig. 1) and HREM images (see Fig. 2). This has been verified by further observation on [011], [111], and [211] orientations, which will be summarized and reported later. Considering that our experiment was conducted at room temperature using the oxygen with low partial pressure in the vacuum, the exclusion of other iron oxides can be explained with the following two items: First, at room temperature Fe_3O_4 is the sole or principal product of the oxidation of Fe [20,21]; second, only FeO and Fe_3O_4 can be readily grown in a high-vacuum environment when oxygen is used as the oxidizing gas [3,4,22]. It was found that the extent and the rate of transformation from Fe_4N to Fe_3O_4 are dependent on the current density of the incident electron beam. Further investigation is needed on the growing rate and thickness of the oxide film with respect to the beam current and irradiation time.

In conclusion, the electron-stimulated oxidization of the Fe_4N nitride inside a transmission electron microscope has been *in situ* observed. The formation of the Fe_3O_4 oxide takes place rapidly when the Fe_4N nitride is exposed to an electron beam, which suggests a new method to prepare Fe_3O_4 film. This process includes the decomposition of the Fe_4N nitride, the desorption of nitrogen from the specimen, and the oxidization of metallic iron by the oxygen survived in the vacuum system.

*Corresponding author.
Electronic address: LIU.Zhiquan@nims.go.jp

[1] Sh. K. Shaikhutdinov, W. Weiss, and R. Schlogl, Appl. Surf. Sci. **161**, 497 (2000).
[2] W. Ranke, M. Ritter, and W. Weiss, Phys. Rev. B **60**, 1527 (1999).
[3] W. Weiss and M. Ritter, Phys. Rev. B **59**, 5201 (1999).
[4] H. C. Galloway, P. Sautet, and M. Salmeron, Phys. Rev. B **54**, R11 145 (1996).
[5] S. A. Chambers, S. Thevuthasan, and S. A. Joyce, Surf. Sci. **450**, L273 (2000).
[6] F. C. Voogt, T. Fujii, P. J. M. Smulders, L. Niesen, M. A. James, and T. Hibma, Phys. Rev. B **60**, 11 193 (1999).
[7] J. F. Anderson, M. Kuhn, U. Diebold, K. Shaw, P. Stoyanov, and D. Lind, Phys. Rev. B **56**, 9902 (1997).
[8] A. V. Mijiritskii, M. H. Langelaar, and D. O. Boerma, J. Magn. Magn. Mater. **211**, 278 (2000).
[9] Y. Gao, Y. J. Kim, S. A. Chambers, and G. Bai, J. Vac. Sci. Technol. A **15**, 332 (1997).
[10] J. M. Heras and L. Viscido, J. Vac. Sci. Technol. A **15**, 2051 (1997).
[11] J. Xu, W. J. Choyke, and J. T. Yates, Jr., J. Appl. Phys. **82**, 6289 (1997).
[12] W. Li, M. J. Stirniman, and S. J. Sibener, J. Vac. Sci. Technol. A **13**, 1574 (1995).
[13] I. Popova, V. Zhukov, and J. T. Yates, Jr., Appl. Phys. Lett. **75**, 3108 (1999).
[14] V. Zhukov, I. Popova, and J. T. Yates, Jr., Phys. Rev. B **65**, 195409 (2002).
[15] Y. Chen, Y. Luo, J. M. Seo, and J. H. Weaver, Phys. Rev. B **43**, 4527 (1991).
[16] Y. Sugimoto, M. Taneya, K. Akita, and H. Kawanishi, J. Appl. Phys. **69**, 2725 (1991).
[17] M. Bouslama, Z. Lounis, M. Ghaffour, M. Ghamnia, and C. Jardin, Vacuum **65**, 185 (2002).
[18] Z. Q. Liu, Z. K. Hei, and D. X. Li, J. Mater. Res. **17**, 2621 (2002).
[19] K. H. Jack, Proc. R. Soc. London A **195**, 34 (1948).
[20] V. S. Smentkowski and J. T. Yates, Jr., Surf. Sci. **232**, 113 (1990).
[21] R. J. Hussey, D. Caplan, and M. J. Graham, Oxid. Met. **15**, 421 (1981).
[22] M. Ritter and W. Weiss, Surf. Sci. **432**, 81 (1999).